Proceedings of FEDSM'98
1998 ASME Fluids Engineering Division Summer Meeting
June 21-25, 1998, Washington, DC, USA

FEDSM98-4901

NUMERICAL SIMULATION OF THE GAS FLOW IN GAS-METAL ATOMIZERS

Pedro I. Espina[1]
Fluid Flow Group
National Institute of Standards and Technology
Gaithersburg, Maryland 20899
Email: pedro.espina@nist.gov

Ugo Piomelli
Department of Mechanical Engineering
University of Maryland
College Park, Maryland 20742
Email: ugo@eng.umd.edu

ABSTRACT

The gas-only flow in a close-coupled, gas-metal atomizer is studied to determine the influence of operational parameters on the structure of the flow field. A parametric study is conducted to determine the effects of jet exit pressure ratio, jet temperature ratio, and base mass-injection on the flows.

Comparisons between Schlieren images and numerical results are found to be in good qualitative agreement; the numerical method predicted the experimental values of base pressure, however, only within 10-20% of the experimental values. Results from the pressure ratio study led to a description of the observed base-pressure behavior on the basis of the resulting jet structure. The temperature ratio results indicated that the industrial practice of gas-heating may be detrimental to the atomization process due to a global reduction of the momentum of the gas flow field. The flow fields obtained with base mass-injection exhibited flow structures similar to those seen in high-speed studies of the liquid metal disruption process. The introduction of mass at the base of the flow has little impact on the flow structure of the surrounding gas flow field.

NOMENCLATURE

a	speed of sound
C_f	friction coefficient, $= 2\,\tau_w/\rho_r a_r^2$
ccw	counter clockwise
k	turbulence kinetic energy
L	length or extension
P	pressure
R	liquid-delivery-tube radius
r	radius or radial coordinate
s	coordinate direction parallel to the exterior surface of the liquid-delivery-tube
T	temperature
$\bar{u}$	mean streamwise velocity
x	axial coordinate
α	angle
ϵ	turbulence dissipation rate
γ	specific heat ratio
ψ	compressible axisymmetric steam function
ρ	density
τ	shear stress
Subscripts	
dt	liquid-delivery-tube
e	annular channel exit
exp	experimental value
jet	annular channel
liq	liquid
max	maximum value
$metal$	property at the melting point of the metal
o	stagnation condition
r	receiving chamber
w	at the wall
Superscripts	
$*$	nondimensional unit (normalized by the receiving chamber property)
$+$	based on wall units

INTRODUCTION

Gas-metal atomization is a process used to transform liquid metal into metal powder. The metal powders produced by this technology exhibit chemical homogeneity and

[1] Address all correspondence to this author.

refined micro-structures, which cannot be obtained by conventional casting techniques. Given their properties, the products made from these powders find widespread applications ranging from jet engine parts to medical implants (Lawley, 1985).

The heart of a gas-metal atomizer is a device called the *atomization nozzle assembly*, which forces the interaction between a high speed gas jet and a liquid stream of molten metal. The interaction between these streams forces an exchange of momentum, which accelerates the liquid and leads to instabilities and disruption of the metal stream. Following disruption, the metal droplets solidify in flight and the resulting powder is separated from the gas.

The atomization nozzle assemblies can be of two types: *free-fall*, or *close-coupled*. In free-fall atomizers (Figure 1, left), the stream of molten metal is allowed to fall unrestricted until it interacts with the gas jet. In close-coupled atomizers (Figure 1, right), the stream of molten metal is delivered by a ceramic conduit (named *liquid-delivery-tube*) to the interaction zone with the gas jets. Close-coupled atomizers are more difficult to operate, but they tend to produce finer powders than free-fall atomizers. Given that the properties of metal powders generally improve with smaller particle sizes (Boettinger *et al.*, 1986), close-coupled atomizers are in high demand and their control is of significant interest to the metal-powder producing industry.

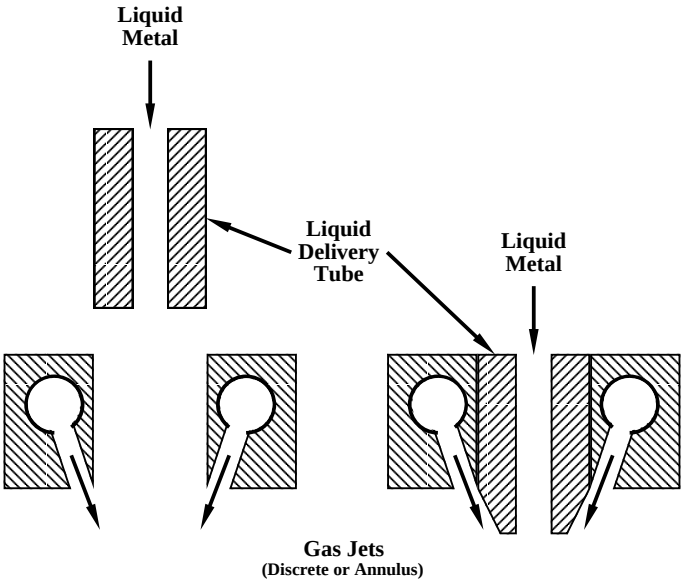

Figure 1. Schematic diagrams of gas metal atomization nozzle assemblies. (Left) free-fall atomizer. (Right) close-coupled atomizer.

The control of a molten stream of metal at a temperature near 1700 K is difficult; historically, this has led to atomization control strategies that predominantly focus on the gas-delivery-system of the atomizers. Initially, gas-only flows were studied experimentally. Couper and Singer (1985) and Ayers and Anderson (1985) determined that the particle-size distribution produced by an atomizer is correlated to the base pressure at the end-face of the liquid-delivery-tube. This reduced base pressure (named *aspiration* pressure by Ayers and Anderson, 1985) was found to be a function of the jet stagnation pressure. Based on these conclusions, Ridder and Biancaniello (1988) postulated the possibility of performing *in situ* particle-size control based on aspiration-pressure control schemes.

Following these experimental findings, research focused on the use of flow models to describe the structure of the gas-only flow, trying to predict the aspiration behavior in atomizers. Various research groups made use of two-dimensional method of characteristics (Espina *et al.*, 1989; Espina, 1991) and wave theory (Ünal, 1989) to predict the structure of the gas jet. Results from these investigations led to phenomenological models describing the aspiration pressure on the basis of the relative location between specific gas jet flow features, and the end-face of the liquid-delivery-tube. Anderson *et al.* (1989) made use of the analogy between the Froude and Mach numbers to study the flow features of the gas-only flow using water bed experiments. Results from these experiments highlighted the similarities between the gas-only flows in atomizers and the flows in truncated plug nozzles used for propulsion.

More recently, research in close-coupled, gas-metal atomization has benefited from the use of Reynolds averaged Navier-Stokes (RANS) solutions. Among other things, this type of research has predicted the separation of the gas wall-jet over the exterior surface of the liquid-delivery-tube – a leading cause of liquid metal freeze-off during atomization (Espina *et al.*, 1993). However, the same results showed the benefits of an increased expansion process over the surface of long liquid-delivery-tubes – a process that, however, can further promote separation. Trying to reconcile these two competing conditions, Espina *et al.* (1993) suggested the use of the longest liquid-delivery-tube that will not lead to separation. In addition, this type of study has documented the use of RANS simulations with: different approximations of the governing equations, turbulence models, and grid adaptation methods (Espina *et al.*, 1993; Figliola *et al.*, 1993; Kuntz and Payne, 1995; Mi *et al.*, 1996; Miller *et al.*, 1996).

Other research groups have used results obtained from RANS simulations as platforms for liquid disruption and particle dynamics studies. Figliola *et al.* (1993) used a solution obtained with a high-Reynolds number k-ϵ turbulence model to predict paths and cooling rates of particles injected through the liquid-delivery-tube into the atomization gas-only flow field. Following this, Kuntz and Payne

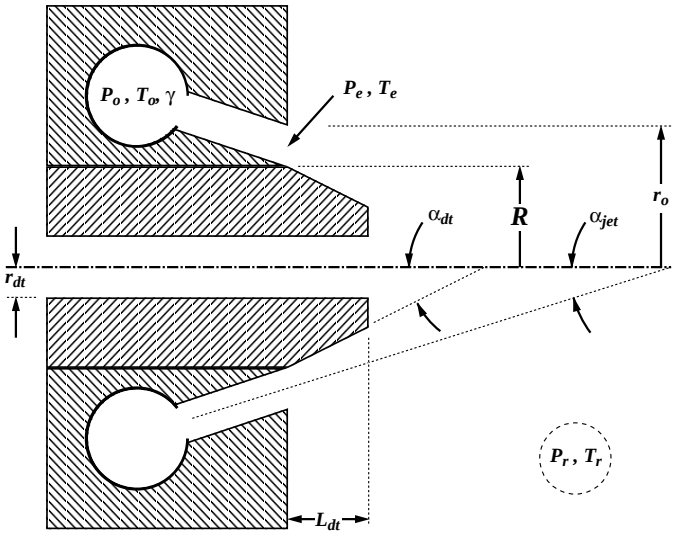

Figure 2. Schematic diagram of the annular jet, close-coupled atomization nozzle assembly studied in this investigation (geometry rotated 90° ccw from its normal operational orientation).

(1995) used a solution obtained with a one-equation turbulence model, in conjunction with a multi-regime empirical disruption model, to predict the full two-phase flow problem in a geometry similar to that used by Ridder and Biancaniello (1988). Kuntz and Payne's results, although the most complex to date, yielded only qualitative agreements with the experimental data due to errors in the gas-only flow solution, lack of physical properties of liquid metal alloys, errors in the empirical, multi-regime disruption model, and decoupling of the gas and liquid phases during the simulations.

The study presented here considers the gas-only flow produced by a generic close-coupled gas-metal atomizer. By "generic", it is implied that the geometry of the atomization nozzle assembly was selected to be representative of numerous designs used by other researchers and industry. The operational parameters are based on those typically used for the production of metal powder (Ayers and Anderson, 1985; Ridder and Biancaniello, 1988). Figure 2 schematically shows the geometry considered, and Table 1 contains a summary of the operational parameters with their typical associated ranges.

Both experimental and numerical results are presented. Experimentally, the atomization gas-only flow is examined using Schlieren photography to identify the position of shock waves, expansion fans, separation lines, and shear layers. These data are used to validate the numerical results over a wide range of conditions. A parametric study is conducted to determine the effects of jet exit pressure ratio,

Table 1. typical parameter ranges used during the operation of the generic gas-metal atomizer in Figure 2.

Parameter	Operational Range	Baseline
R		4.825 mm
r_o/R		1.0632
α_{jet}	$0° \rightarrow 27.5°$	22.5°
α_{dt}	$0° \rightarrow 27.5°$	22.5°
L_{dt}/R	$0 \rightarrow 0.6$	0.6
r_{dt}/R	$0.21 \rightarrow 0.31$	0.31
gas specie	Ar, He, or N_2	Ar
P_r		1 atm
P_e/P_r	$3.8 \rightarrow 53.5$	33
T_r		293 K
T_e/T_r	$0.65 \rightarrow 1.31$	0.65

jet temperature ratio, and base mass injection (which is intended to model the presence of the liquid phase). Based on these results, it is concluded that, with some experimental verification, parameterization studies such as this can be a very cost effective way to optimize this industrial process.

NUMERICAL METHOD

Governing Equations

The axisymmetric, steady, compressible flow in a close-coupled, gas-metal atomizer is governed by the non-reacting Navier-Stokes equations. In this work, the Navier-Stokes equations are solved in strong, conservative form in a curvilinear coordinate system (Pulliam and Steger, 1980). The fluid is assumed to be a thermally- and calorically-perfect gas that exhibits a Newtonian stress-strain behavior. The dimensionless thermal conductivity is taken to be identical to the dimensionless molecular viscosity, which is related to the static temperature by the Sutherland viscosity law.

Numerical Algorithm

The solution to the Navier-Stokes equations was accomplished using the NPARC code (Cooper and Sirbaugh, 1989), which is a descendant of the NASA ARC2D code (Pulliam and Steger, 1980). In this implementation of the Beam-Warming (1976) approximate factorization algorithm, time advancement is performed using a backward Euler scheme. Second-order central differences are used to approximate spatial derivatives and approximate factoriza-

tion is used to facilitate solution of the resulting system of equations. Both second- and fourth-order artificial dissipation are introduced to suppress dispersion errors near shock waves and decoupling of even-odd modes due to the central difference discretization. The resulting equations yield a series of block pentadiagonal systems that can be linearized by time-advancing the viscous fluxes and the axisymmetric source terms explicitly. This results in a series of scalar pentadiagonal systems that are solved directly using the Thomas algorithm.

Turbulence Model

Solutions to the atomization gas-only flows were obtained using a compressible implementation (Georgiadis *et al.*, 1994) of Chien's (1982) k-ϵ turbulence model. However, in this investigation, the value of the $C_{\epsilon 1}$ constant in Chien model was reduced 10% to correct for an overprediction in the production of turbulence kinetic energy dissipation observed in supersonic base flows (Espina and Piomelli, 1997).

In the NPARC code, the solution of the turbulence equations is time-lagged with respect to the solution of the flow equations and was accomplished using the algorithm suggested by Sahu and Danberg (1986). In this algorithm, second-order, upwind differences are used to approximate the spatial derivatives, and approximate factorization is used to facilitate solution of the resulting equation. This renders the use of artificial dissipation unnecessary, given the inherent smoothing properties of the upwind differences. The resulting equation yields a series of block tridiagonal systems that are solved directly using a block version of the Thomas algorithm.

Physical Domain and Boundary Conditions

The computational domain used in this investigation (see Figure 3) follows the specifications of the close-coupled atomizer used by Ridder and Biancaniello (1988). However, it changes their discrete jet geometry to an annular jet version with the same total cross-sectional area. The computational domain was segmented into three separate blocks: block 1 is the annular channel (discretized using 42×41 points in the axial and radial directions respectively), block 2 is the volume over the liquid-delivery-tube (a ring-shaped volume extending radially outward from the liquid-delivery-tube external diameter and bound in the axial direction by the liquid-delivery-tube end; 57×161 grid points were used), and block 3 is the volume after the axial-end of the liquid-delivery-tube (289×215). Blocks 2 and 3 extend radially to a distance of $10R$, while block 3 extends axially to a distance of $14.7R$ from the exit-plane of the annular channel.

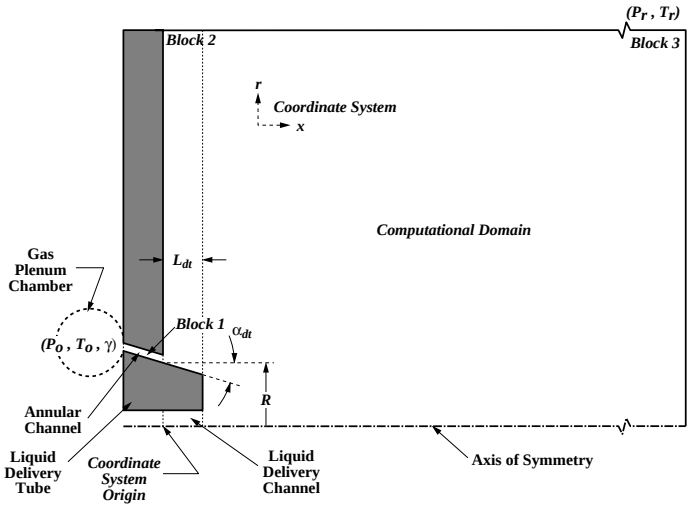

Figure 3. Schematic diagram of the computational domain used to model the gas-only flow in a close-coupled atomizer.

Within each block, the mesh points were distributed using the SAGE grid adaptation program (Davies and Venkatapathy, 1992). At all solid boundaries, the first line of points parallel to the wall was forced to be located at $y^+ \simeq 1$ to obtain accurate resolution at the wall layer. Through doubling the number of point in each direction it was determined that the previously mention resolutions were adequate to render grid independent solutions. As an example, Figures 4 shows one of the final adapted grids used.

Characteristic-type boundary conditions were used at the inlet of the annular channel (P_o, T_o specified) and at the free boundaries of blocks 2 and 3 (P_r, T_r specified). The block 1 $\rightleftharpoons$ block 2 interface as well as the

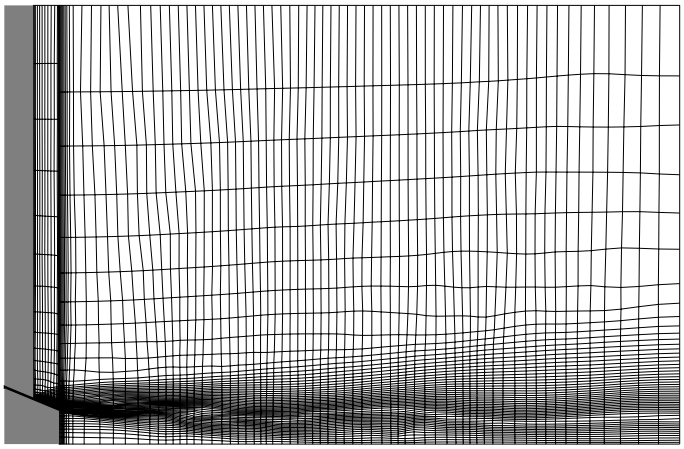

Figure 4. Typical computational mesh adapted for simulation of gas-only flow in a close-coupled gas-metal atomizer (only every fourth grid line is shown for clarity).

block 2 $\rightleftharpoons$ block 3 interface were interpolated explicitly. Axisymmetry was used at the axis of the third block while all other boundaries were treated as adiabatic, non-slip walls.

Additional details regarding the various aspects of the numerical method here used can be found in Espina and Piomelli (1997), and Espina (1997).

RESULTS

Some of the parameters listed in Table 1 are typically fixed by the design of the atomization nozzle assembly: R, r_o/R , α_{jet}, and α_{dt}. Others can be changed prior to the initiation of the atomization process: L_{dt}/R, r_{dt}/R, and the gas specie. However, a number of parameters can be changed *in situ*, providing the ability to modify the atomization process output based on some product quality measurement: P_r, P_e/P_r, T_r, and T_e/T_r. In this section, we study the effects of both jet pressure and temperature ratios on the structure of the gas-only atomization flow produced by the geometry shown in Figure 2, and we explore the effects of the liquid on the gas flow by modeling the atomization flow with base mass injection. Such knowledge can be of assistance in the design of atomizers and in the development of control strategies for them.

Effects of Jet Pressure Ratio

In this section we investigate the effects of jet pressure ratio on the structure of the gas-only flow. We chose to model five jets at pressure ratios of P_e/P_r = 6.6, 20, 33, 46, and 53 (although only the lower four pressure ratio jets are discussed in detail due to the similarities between the P_e/P_r = 46 and 53 jets). Density contours are compared to Schlieren images in Figure 5. Overall, good agreement can be observed between experimental data and numerical results; the flow structures (shock waves, expansion fans, shear layers) observed in the experiments are also present in the calculations, and their locations are generally correct.

At all pressure ratios a large number of features in these close-coupled atomization flows are similar. Initially, the gas accelerates from a quasi-stagnated state to sonic conditions along the length of the annular channel. At the exit of the channel, the flow emerges with a pressure higher than the receiving-chamber pressure and forms an underexpanded wall jet over the outer surface of the liquid-delivery-tube. Depending on the pressure ratio, this wall jet separates somewhere along the surface of the liquid-delivery-tube forming an annular underexpanded jet that entraps a volume of fluid at the base of the liquid-delivery-tube. The resulting base flow has characteristics similar to those seen in other axisymmetric supersonic base flows (Espina and

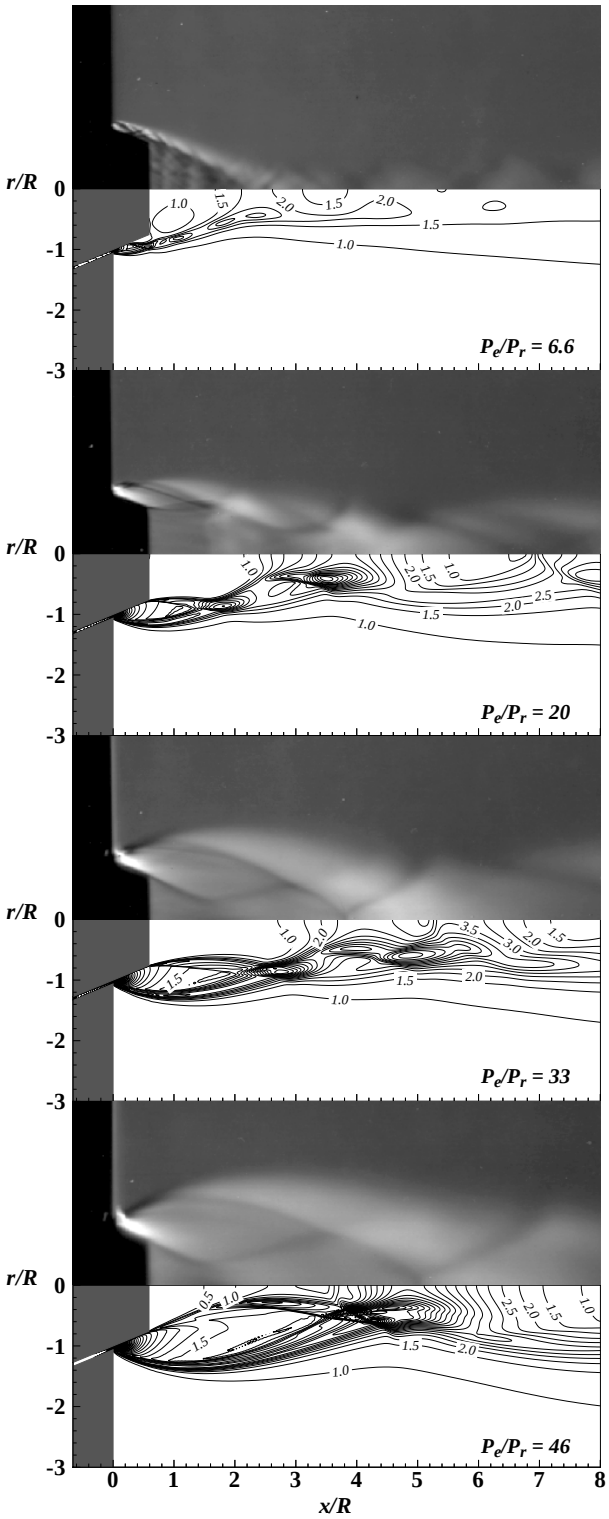

Figure 5. Effects of jet pressure ratio on the structure of gas-only atomization flows (baseline settings except as noted): experimental schlieren pictures (upper images), numerical density distributions, $\rho^* = \rho/\rho_r$ (lower images): $\Delta\rho^* = 0.5$.

Piomelli, 1997). At the end of the separation region, the jet flow looses its annular character and becomes a single supersonic jet. This jet continues downstream through a series of barrel-shocks[2] until it looses enough momentum to become subsonic.

At $P_e/P_r \simeq 6.6$ (top image in Figure 5), the annular portion of the jet displays multiple barrel-shocks before its transformation into a single jet at $x/R \simeq 2.05$. Upon its separation from the surface of the liquid-delivery-tube, the annular flow encapsulates a conically shaped region at the base of the liquid-delivery-tube. This entrapped flow draws momentum from the main flow across the inner shear layer, leading to relatively fast recirculating velocities inside of it ($M_{max} \simeq 0.76$). After its transformation into a single jet at $x/R \simeq 2.05$, the gas continues downstream as a supersonic jet for some distance (at least up to $x/R = 8$). The outer shear layer entrains little surrounding fluid and the jet shows little spreading, attaining a maximum radius of only $1.2\,R$ by $x/R = 8$.

For a pressure ratio of 20 (second image from the top in Figure 5) the annular portion of the flow also contains multiple barrel-shocks: a complete one, followed by the initial portion of a second one. The middle portion of the initial barrel-shock pinches the separation streamline, giving it an hourglass shape. The flow reattaches at $x/R \simeq 2.80$, when the second barrel-shock reaches the axis of symmetry. The outer shear layer draws about twice as much fluid from its surroundings as the $P_e/P_r \simeq 6.6$ jet (Espina, 1997). This high entrainment, combined with a jet mass flow-rate that is three times larger than the mass of the $P_e/P_r \simeq 6.6$ jet, yields a thicker jet with a maximum radius of $1.5\,R$ at $x/R = 8$

The baseline jet, $P_e/P_r \simeq 33$ (third image from the top in Figure 5), also shows a complete barrel-shock followed by a partial one in the annular portion of the flow ($x/R < 3.65$). For this pressure ratio, the arrangement of the annular barrel-shocks places the middle portion of the initial one near the center of the separation bubble, leading to a longer and narrower separation region than those seen before. At this pressure ratio the annular wave structure persists beyond the reattachment point, changing to a single-jet wave structure at $x/R \simeq 5.2$. For this pressure ratio, the flow entrainment is reduced compared to that seen in the $P_e/P_r \simeq 20$ jet (Espina, 1997). The lower entrainment yields a jet with a maximum radius of $1.7\,R$ (at $x/R = 8$), even though the jet carries 65% more mass than its lower pressure ratio counterpart.

The structure of the high pressure ratio jet, $P_e/P_r \simeq 46$ (bottom image in Figure 5), is different in many ways from the lower pressure ratio cases. At this pressure ratio, the annular flow only contains one barrel-shock with its central portion forcing the inner shear-layer very close to the axis of symmetry. This leads to a short, conically shaped separation bubble ($x/R < 2$) with a small surface area that allows for little momentum flux across the inner shear layer. At this pressure ratio the entrainment increases, drawing as much surrounding fluid as the $P_e/P_r \simeq 20$ jet (Espina, 1997). The additional entrainment, combined with a 28% increase in mass flow over the $P_e/P_r \simeq 33$ jet levels, leads to a maximum radius of $2\,R$, at $x/R = 8$. However, at this distance, the jet spreading rate is still under the strong local influence of the wave structures, and this radius is a function of the inviscid flow structure as much as it is a function of the flow entrainment.

Figure 6 shows the aspiration pressure as a function of the jet pressure ratio. The experimental results, which are typical of this type of atomizer (Ayers and Anderson, 1985; Ting and Grant, 1986; Ridder and Biancaniello, 1988; Anderson *et al.*, 1989), were recorded in the experimental facility used by Espina (1991). At each point, the experimental uncertainty of the data is no larger than the size of the symbols used in the plot.

At low pressure ratios, $P_e/P_r < 5$, the liquid-delivery-tube experiences a high aspiration pressure, $P_{dt}/P_r > 1$, that can lead to a "blow-back" condition (*i.e.,* gas flowing into the liquid-delivery-tube and bubbling through the liquid metal in the crucible, generally leading to a freeze-off). For mid-range pressure ratios, $5 < P_e/P_r < 25$, the

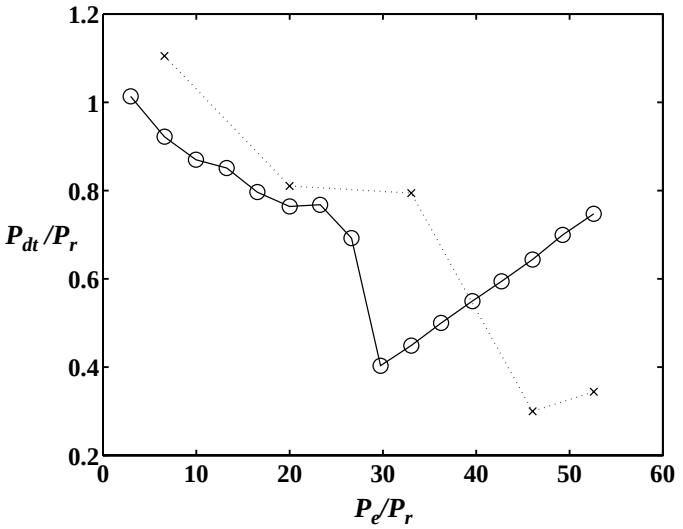

Figure 6. Effect of jet pressure ratio, P_e/P_r, on aspiration pressure, P_{dt}/P_r, for the selected close-coupled atomization nozzle assembly (baseline settings except as noted). —○— : experimental data, $P_{r_{exp}} = 98.574\,kPa$; —×— : numerical results.

[2] A "barrel-shock" is a repetitive barrel-shaped flow structure initiated by an expansion fan and terminated by an oblique shock wave. The resulting flow pattern is often seen in supersonic jets as a series of diamonds (John, 1984).

liquid-delivery-tube records ever decreasing aspiration pressures that plateau near $P_e/P_r \simeq 20$. For a narrow range of pressure ratios thereafter, $25 < P_e/P_r < 30$, the aspiration pressure decreases rapidly, leading to its minimum value, or *maximum aspiration condition*. Further increases in jet pressure ratio lead to linear increases in aspiration pressure, eventually leading to a second blow-back regime.

The numerical calculations generally miss the prediction of the aspiration pressure by 10-20% [a result consistent with similar numerical data obtained from supersonic base flow simulations (Espina and Piomelli, 1997; Espina, 1997)]. The initial decay in the numerical results is shifted towards higher values of jet pressure ratio as an effect of the incorrect prediction of the velocity field in the recirculation region. However, the simulations capture accurately the trends observed in the experimental data, as shown by the sudden decrease in aspiration pressure at the maximum aspiration condition, followed by a gradual increase as the pressure ratio is further increased (see Figure 6).

An important feature of these jets is that flow separation may occur over the outer surface of the liquid-delivery-tube for some conditions (see Figure 7). The occurrence of separation, which is a function of jet pressure ratio and liquid-delivery-tube extension, has been suggested (Ridder *et al.*, 1992) to cause liquid metal to be drawn from the end-face of the liquid-delivery-tube into its outer surface, where it is exposed to the very cold expanding gas of the annular wall jet. The extreme temperature difference between the metal and the gas promotes the solidification and accumulation of metal, leading to a shape alteration of the liquid-delivery-tube. Typically, this sequence of events induces a freeze-off that ends the atomization process prematurely. Therefore, this separation is detrimental to the process of gas-metal atomization and should be avoided at all costs.

Figure 8 shows the skin friction coefficient, C_f, over the surface of the liquid-delivery-tube as a function of surface distance, $s = x/cos(\alpha_{dt})$, for four pressure ratios. At all pressure ratios, the friction coefficient increases early in the length of the liquid-delivery-tube due to the flow acceleration caused by the expansion fan emanating from the end-lip of the annular channel (see Figure 7). From there on, the friction coefficient decays smoothly as the wall jet boundary layer loses momentum to friction.

For a low pressure ratio, $P_e/P_r \simeq 6.6$, the simulation predicts that the flow will separate at $s/R \simeq 0.24$, while for intermediate pressure ratios, $P_e/P_r \simeq 20$ and 33, the separation takes place in the neighborhood of $s/R \simeq 0.6$. At the high pressure ratio ($P_e/P_r \simeq 46$) the flow never separates before the end of the liquid-delivery-tube. Near the end of the liquid-delivery-tube, furthermore, the friction coefficient increases rapidly due to the second expansion fan that forms at the end-corner of the liquid-delivery-tube.

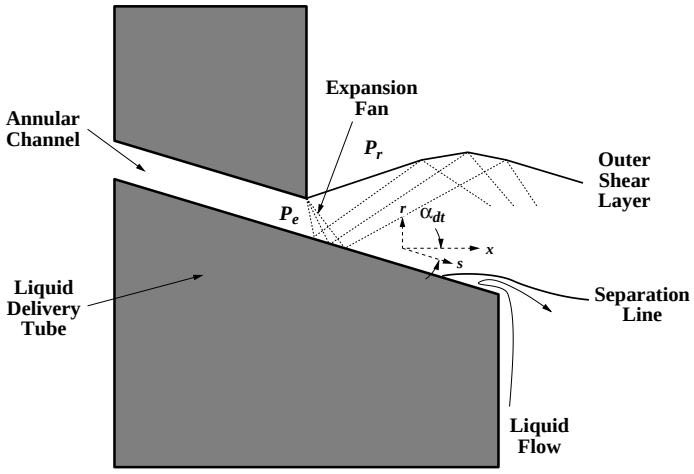

Figure 7. Schematic diagram of the separation phenomenon at the end of the liquid-delivery-tube.

The observed behavior leads to the following model of the aspiration phenomenon that describes the trend experimentally, shown in Figure 6. For mid-range pressure ratios, $P_e/P_r < 20$ (decreasing P_{dt}/P_r range), the flow over the liquid-delivery-tube separates early on along its trajectory over the liquid-delivery-tube. In this range, the decrease in aspiration pressure with increasing jet pressure ratio results from an ever larger expansion level due to the increasing underexpansion of the wall jet (*i.e.,* as the pressure ratio in-

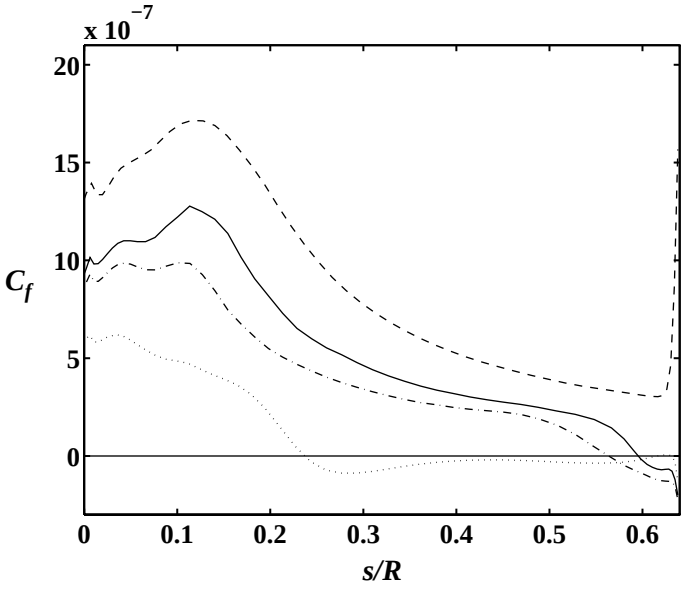

Figure 8. Effect of jet pressure ratio on flow separation over the liquid-delivery-tube (baseline settings except as noted): $C_f = 2\,\tau_w/\rho_r a_r^2$. ·····: $P_e/P_r \simeq 6.6$; -·-·-: $P_e/P_r \simeq 20$; ——: $P_e/P_r \simeq 33$; - - -: $P_e/P_r \simeq 46$.

creases the separation point moves downstream allowing for more expansion in the wall jet and thus, lower pressures in the flow encapsulating the base region). At pressure ratios between 20 and 25 (plateau in P_{dt}/P_r range), the flow separates close to the end of the liquid-delivery-tube, leading to an aspiration pressure level that is controlled by the dynamics of the flow in the hourglass shaped separation bubble. Given that the structure of the hourglass shaped separation bubble does not change significantly in this pressure ratio range, then it follows that the aspiration pressure remains fairly constant. For higher pressure ratios, $P_e/P_r > 25$ (increasing P_{dt}/P_r range), the flow never separates from the face of the liquid-delivery-tube and a second expansion fan forms at its end-corner. This second expansion controls both the shape of the separation region and the aspiration pressure. The higher the pressure ratio goes, the higher the pressure before the second expansion process will be. Given that the turning angle at the end of the liquid-delivery-tube is constant, the second expansion process will yield ever smaller separation regions with ever increasing aspiration pressures.

Effects of Jet Temperature Ratio

In some metal-powder production facilities, the gas supply is pre-heated[3] in an attempt to decrease the thermal shock that the ceramic liquid-delivery-tube experiences as a consequence of its contact with the hot liquid metal and the cold gas wall-jet. The practice of gas pre-heating, although expensive and difficult to implement, has also been justified on the basis that it increases the energy available in the gas to disrupt the metal liquid. Thus, it could lead to the formation of finer powders. In this section, we examine the effects of jet stagnation temperature by comparing the baseline atomization-flow calculation (see Table 1) with a similar one in which the gas is at a stagnation temperature twice as high.

Figure 9 compares the density distributions of the unheated, baseline flow ($T_e/T_r = 0.65$) with the heated ($T_e/T_r = 1.31$) atomization flow. As expected, the basic structure of the jet remains unchanged, given that it is controlled by the inviscid portion of the flow, which is only a function of the jet pressure ratio. The density of the heated flow, however, changes in a manner inversely proportional to the change in temperature (*i.e.,* $\rho_{hot}/\rho_{cold} = T_{cold}/T_{hot} = 1/2$); given that the Mach number distribution remains unchanged and that the speed of sound scales with the square root of the stagnation temperature, the speed of the fluid only increase proportionally to the square root of the temperature increase (*i.e.,*

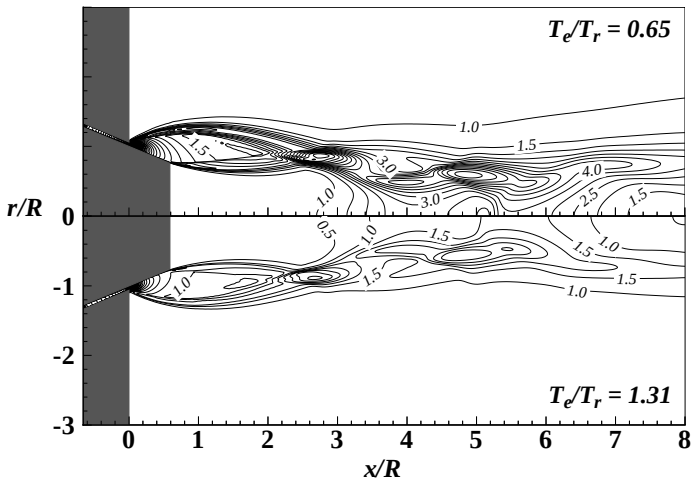

Figure 9. Effects of jet temperature ratio on the density distribution, ρ^*, of gas-only atomization flows (baseline settings except as noted): $\Delta\rho^* = 0.5$.

$|V|_{hot}/|V|_{cold} = \sqrt{T_{hot}/T_{cold}} = \sqrt{2/1}$). This leads to a net loss of momentum in the flow field of 29% (*i.e.,* $1 - \sqrt{2}/2$), probably reducing the ability of the hot flow to disrupt the liquid metal effectively.

The heated jet appears to entrain about 33% more fluid than the unheated jet, even though it carries 29% less mass than its unheated counterpart (Espina, 1997). The increased entrainment is not sufficient to boost the jet spreading rate of the hot flow, whose diameter is 32% smaller by $x/R \simeq 8$ than that of the unheated jet.

The higher temperature, furthermore, appears to lead to earlier separation of the wall jet over the liquid-delivery-tube. Figure 10 shows how the hot gas flow does not experience the increase in skin friction velocity early in the length of the liquid-delivery-tube that the unheated jet displayed. Overall, the hot wall jet, with its lower momentum, imposes less drag on the surface of the liquid-delivery-tube than the unheated jet. However, the lower momentum available in the hot jet leads to its early separation at $s/R = 0.52$.

The higher stagnation temperature does improve the thermal conditions over the surface of the liquid-delivery-tube. Doubling the stagnation temperature yields an almost constant doubling of the temperature distribution over the liquid-delivery-tube. Given the disparity in temperatures inside and outside of the ceramic liquid-delivery-tube, this wall temperature increase could improve the structural integrity for some ceramic materials with good erosion properties but deficient thermal shock properties (characteristics often encountered among the materials used to manufacture liquid-delivery-tubes).

[3]Gas stagnation temperatures as high as $700K$ are typical in industrial atomization facilities.

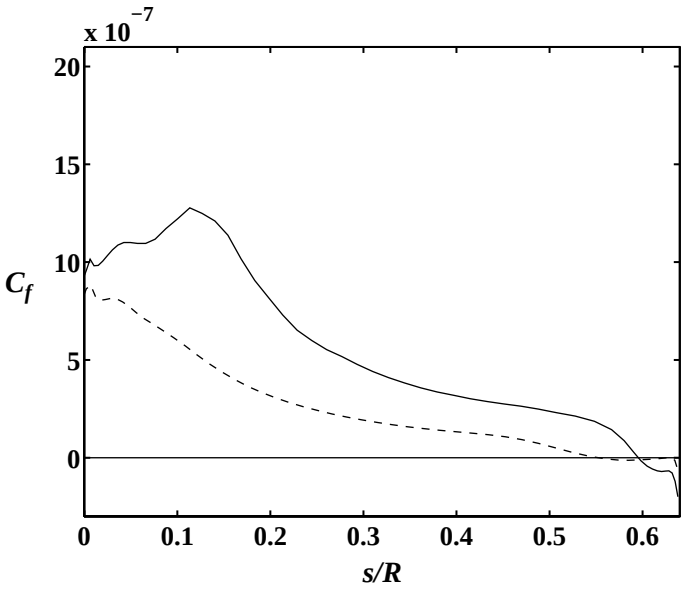

Figure 10. Effect of jet temperature ratio on flow separation over the liquid-delivery-tube (baseline settings except as noted): $C_f = 2\,\tau_w/\rho_r a_r^2$. ——: $T_e/T_r = 0.65$; - - -: $T_e/T_r = 1.31$.

Effects of Base Mass Injection

The physics of liquid disruption are not well understood and this makes the numerical simulation of the full gas-metal atomization phenomenon nearly impossible at present. However, the introduction of the dense liquid metal at the base of the liquid-delivery-tube will undoubtedly change the character of the gas-only atomization flows described in the previous sections. In this section, we investigate the effects that the liquid metal flow may have on the atomization flow by injecting mass at the base of the liquid-delivery-tube in the form of a hot gas stream (*i.e.*, $T = T_{metal} \simeq 1650\ K$) introduced through the liquid-delivery-tube channel (see Figure 3).

Nickel-based super alloys have liquid densities that are approximately 4500 times larger than the density of argon at standard conditions. This disparity in density makes it impossible to match exactly the parameters of the liquid metal/gas interaction using argon as a surrogate fluid. However, observing that the liquid is drawn into the atomization process at a very low velocity ($\bar{u}_{liq} \simeq 1.2\ m/s$), it is possible to investigate the injection effects using a gas injection-velocity that yields the same momentum-flux as the liquid. For the baseline flow, the injection rate that yields such conditions is $\dot{m}_{dt}/\dot{m}_{jet} = 0.0013$. An additional calculation was performed injecting almost three times as much gas into the base of the flow ($\dot{m}_{dt}/\dot{m}_{jet} = 0.0041$).

Contours of the compressible axisymmetric stream function for three cases (the baseline flow and the two mass-injection rates described above) are shown in Figure 11. At

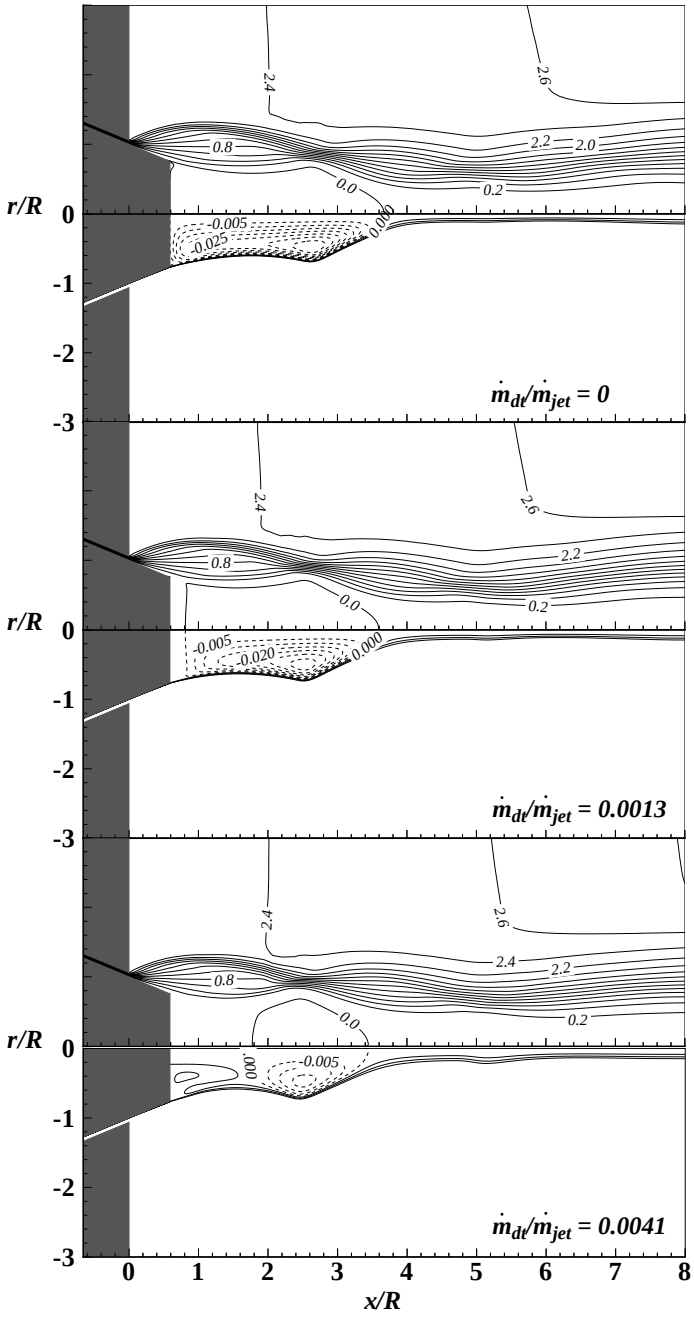

Figure 11. Effects of liquid-delivery-tube mass injection on the compressible axisymmetric stream function distribution, $\psi^* = \psi/\rho_r a_r R$, of gas-only atomization flows (baseline settings except as noted): $\Delta\psi^* = 0.2$ (upper images), $\Delta\psi^* = -0.005$ (lower images).

the lower mass-injection rate (second image from the top in Figure 11), the additional fluid pushes the upstream portion of the separation bubble downstream, moving the first stagnation point away from the base of the liquid-delivery-tube

to an axial distance of $x/R \simeq 0.8$. The addition of mass has little effect on the surrounding annular jet flow; the end of the separation bubble is located nearly at the same place as in the baseline flow (top image in Figure 11). The resulting reduction in the surface area of the separation bubble leads to the deceleration of the flow inside it due to a reduction in the area available for momentum transfer across the inner shear-layer. The additional fluid is rapidly entrained by the inner shear-layer (before $x/R \simeq 1$) and thereafter the flow remains almost unaffected by the mass injection.

The impact of a mass injection rate almost three times larger was also tested. The results of this simulation are shown at the bottom of Figure 11. At this rate of injection, the first stagnation point at the near-side of the separation bubble moves further downstream to an axial location of $x/R \simeq 1.8$. The resulting separation bubble is smaller than that seen at the lower injection rate and this leads to even slower recirculation velocities inside it. As before, the inviscid flow of the annular jet continues to dominate the shape and location of the far-side of the bubble which remains undisturbed. The streamline labeled $\psi^* = 0.005$ (Figure 11 bottom) shows that at this injection rate, the injected flow has enough momentum to form a hot jet, of radius r_{dt}, which propagates from the end of the liquid-delivery-tube to the first separation point. At this location, the hot jet is drawn into the inner shear-layer by its lower pressure and it is then absorbed into the main flow stream.

The injected flow bounded by the $\psi^* = 0$ and $\psi^* = 0.005$ streamlines has a mushroom-like shape similar to that seen in high-speed movies of the liquid flow during atomization (Ridder *et al.* 1992). This may indicate that a recirculation bubble, similar to the one seen in the flow at the bottom Figure 11, may remain present during gas-metal atomization. This separation bubble would then be directly responsible for providing a lift force to the drawn liquid column, which is directly responsible for its radial spreading. Without this phenomena, the metal would remain as a narrow stream flow for a longer distance decreasing the gas-liquid interaction area, and thus leading to less efficient disruption dynamics. Finally, it is observed from these simulations that neither mass injection rate appeared to modify the gas wall jet flow over the liquid-delivery-tube in any significant way.

CONCLUSIONS

The gas-only flow fields in close-coupled gas-metal atomizers were computed using methodologies previously tested in similar configurations (Espina and Piomelli, 1997). Simulations were carried out to determine the effects of jet pressure ratio, gas pre-heating and base mass-injection on the gas-only atomization flow.

Five jet pressure ratios were selected, $P_e/P_r = 6.6$, 20, 33, 46, 53. The numerical results showed that, although the aspiration pressure was not predicted with satisfactory accuracy, the resulting jet structure was in good qualitative agreement with experimental Schlieren pictures. The wall jet flowing over the liquid-delivery-tube separated for a certain set of conditions leading to a possible freeze-off condition. Given the severe consequence of flow separation over the liquid-delivery-tube for the atomization process, it is advisable to make use of short liquid-delivery-tubes to avoid flow separation. The separation behavior seen, in conjunction with the observed jet structure, lead to a phenomenological model which describes the aspiration behavior observed experimentally. Our results suggest that the operation of the atomizer in the increasing P_{dt}/P_r range reduces the chances of separation at the end of the liquid-delivery-tube, thus avoiding the costly possibility of a freeze-off.

The effects of gas heating were studied to determine the effects of this industrial practice on the gas-only atomization flow. Heated jets were shown to have less momentum than their unheated counterparts, which suggests that heating may be detrimental to the formation of fine metal powder. The additional heat was shown to lead to early separation over the surface of the liquid-delivery-tube. In addition, it was shown that increasing the jet temperature ratio leads to a proportional increase in the gas temperature that may improve conditions to avoid thermal shock of the liquid-delivery-tube material. In our opinion, however, the practice of gas-heating should be avoided unless the need to preserve the structural integrity of the liquid-delivery-tube material absolutely requires it.

The effects that the liquid flow may have on the gas during atomization were studied by modeling the gas-only flow with hot gas mass injection at the base of the liquid-delivery-tube. Two rates of injection were tested: one matching the momentum flux of the liquid, and the other having a mass flow almost three times as large as the first. The injected flow took the form of a jet projecting out of the base of the liquid-delivery-tube, which then blossomed into a mushroom-shaped structure similar to that seen in the liquid metal via high-speed movies of the atomization process. Neither of the injection rates studied appeared to change the structure of the outer gas-only flow.

ACKNOWLEDGMENT

This investigation was sponsored by the Chemical Science and Technology Laboratory of the National Institute of Standards and Technology (NIST). Computational support was provided by the High Performance Systems and Service Division at NIST. The authors thank Drs. George

E. Mattingly and Gregory J. Rosasco for their support. The contributions of and Dr. Stephen D. Ridder, and Ms. Francis S. Biancaniello are gratefully acknowledged.

REFERENCES

Anderson, I. E., Morton, H., and Figliola, R. S., 1989, "Fluid Flow Effects in Gas Atomization Processing," *Physical Chemistry of Powder Metals: Production and Processing*, W. M. Small, ed., TMS, pp. 229–249.

Ayers, J. D., and Anderson, I. E., 1985, "Very Fine Metal Powders," *JOM*, Vol. 37, No. 8, pp. 16–21.

Beam, R., and Warming, R. F., 1976, "An Implicit Finite Difference Algorithm for Hyperbolic Systems in Conservation Law Form," *J. Comp. Phys.*, Vol. 22, No. 1, pp. 87–110.

Boettinger, W. J., Bendersky, L., and Early, J. G., 1986, "An Analysis of the Microstructure of Rapidly Solidified Al-8 Wt. Pct. Fe Powder," *Met. Trans. A*, Vol. 17, No. 1, pp. 781–790.

Chien K.-Y., 1982, "Predictions of Channel and Boundary-Layer Flows with a Low-Reynolds-Number Turbulence Model," *AIAA J.*, Vol. 20, No. 1, pp. 33–38.

Cooper, G. K., and Sirbaugh, J. R., 1989, "PARC Code: Theory and Usage," AEDC–TR–89–15, Arnold Engineering Development Center, Arnold AFB, TN.

Couper, M. J., and Singer, F., 1985, "Rapidly Solidified Aluminum Alloy Powder Produced by Optimization of the Gas Atomization Technique," *Rapidly Quenched Metals*, S. Steeb and H. Warlimont, eds., Amsterdam, Netherlands, pp. 1737.

Davies, C. B. and Venkatapathy, E., 1992, "Application of a Solution Adaptive Grid Scheme to Complex Three-Dimensional Flows," *AIAA J.*, Vol. 30, No. 9, pp. 2227–2233.

Espina, P. I., Ridder, S. D., Biancaniello, F. S., and Mattingly, G. E., 1989, "Aerodynamic Analysis of the Aspiration Phenomena in a Close-Coupled Inert Gas Atomizer", *Characterization & Diagnostics of Ceramics & Metal Particulate Processing*, E. J. Lavernia *et al.*, eds., TMS, pp. 49–62.

Espina, P. I., 1991, "An Investigation of the Compressible Flow in a Supersonic Inert Gas-Metal Atomizer," Master Thesis, University of Maryland, College Park, MD.

Espina, P. I., Piomelli, U., and Mattingly, G. E., 1993, "A Numerical Investigation of the Compressible Flow Field Produced in an Annular Jet, Close-Coupled, Gas Metal Atomizer," *Computational and Numerical Techniques in Powder Metallurgy*, D. Madam, *et al.*, eds., TMS, pp. 41–53.

Espina, P. I., and Piomelli, U., 1997, "A Validation of the NPARC Code in Supersonic Base Flows," AIAA Paper, 97–0032.

Espina, P. I., 1997, "Study of an Underexpanded Annular Wall Jet Past an Axisymmetric Backward-Facing Step," Ph.D. Dissertation, University of Maryland, College Park, MD.

Figliola, R. S., and Anderson, I. E., 1993, "Characterization of High Pressure Gas Atomization Flow Fields," *Computational and Numerical Techniques in Powder Metallurgy*, D. Madam, *et al.*, eds., TMS, pp. 29–39.

Georgiadis, N. J., Chitsomboon, T., and Zhu, J., 1994, "Modification of the Two-Equation Turbulence Model on NPARC to a Chien Low Reynolds Number k-ϵ Formulation," NASA TM–106710.

John, J. E. A., 1984, *Gas Dynamics*, 2nd edition, Allyn and Bacon, Inc, Boston, pp. 161–162.

Kuntz, D. W., and Payne, J. L., 1995, "Simulation of Powder Metal Fabrication with High Pressure Gas Atomization," *Advances in Powder Metallurgy and Particulate Materials, Part 1: Powder Production and Characterization*, M. Phillips and J. Porter, ed., MPIF, pp. 63–78.

Lawley, A., 1985, "Powder Metallurgy and Rapid Solidification – Compelling Technologies," *JOM*, Vol. 37, No. 8, pp. 15.

Mi, J., Figliola, R. S., Anderson, I. E., 1996, "A Numerical Simulation of Gas Flow Field Effects on High Pressure Gas Atomization Due to Operating Pressure Variation," *Mat. Sci. Eng.*, Vol. A208, No. 1, pp. 20–29.

Miller, R. S., Miller, S. A., Savkar, S. D., and Mourer, D. P., 1996, "Two Phase Flow Model for the Close-Coupled Atomization of Metals," *Int. J. of Powder Met.*, Vol. 32, No. 4, pp. 341–352.

Pulliam, T. H., and Steger, J. L., 1980, "Implicit Finite-Difference Simulation of Three-Dimensional Compressible Flows," *AIAA J.*, Vol. 18, No. 2, pp. 159–167.

Ridder, S. D., and Biancaniello, F. S., 1988, "Process Control During High Pressure Atomization," *Mat. Sci. Eng.*, Vol. 98, pp. 47–51.

Ridder, S. D., Osella, S. A., Espina, P. I., and Biancaniello, F. S., 1992, "Intelligent Control of Particle Size Distribution During Gas Atomization," *Int. J. of Powder Met.*, Vol. 28, No. 2, pp. 133–138.

Sahu, J., and Danberg, J. E., 1986, "Navier-Stokes Computations of Transonic Flows with a Two-Equation Turbulence Model," *AIAA J.*, Vol. 24, No. 11, pp. 1744–1751.

Ting, E. Y., and Grant, N. J., 1986, "Metal Powder Production by Gas Atomization," *Progress in Powder Metallurgy*, MPIF, Vol. 41, pp. 67–86.

Ünal, A., 1989, "Gas Flow in Atomization Nozzles," *Physical Chemistry of Powder Metals: Production and Processing*, W. M. Small, ed., TMS, pp. 201–228.